Journal of Applied Fluid Mechanics, Vol. 10, No. 1, pp. 447-458, 2017.
Available online at www.jafmonline.net, ISSN 1735-3572, EISSN 1735-3645.
DOI: 10.18869/acadpub.jafm.73.238.26974

Numerical Study of Unsteady Cavitating Flows around a Hydrofoil

A. Bel Hadj Taher†, H. Kanfoudi, M. Ennouri and R. Zgolli

Laboratory of Hydraulic and Environmental Modeling, National Engineering School of Tunis, University of Tunis El Manar, 1002 Tunis, Tunisia.

†*Corresponding Author Email: Ahmed.lmhe_enit@yahoo.fr*

(Received July 21, 2016; accepted August 24, 2016)

ABSTRACT

In this paper, we report the results of a numerical investigation on unsteady cavitating flows around a circular leading edge (CLE) hydrofoil. The objective of this study is to properly predict the appearance of cavitation pocket, its development and its detachment causing adverse effects on industrial systems such as microscopic plastic deformations at the solid walls. For this reason it is very important to study the influence of turbulence models on simulation results. We present a closing of the hydrodynamic equation system by a transport equation of an active scalar (volume fraction of the vapor phase) with a source terms. The Computational Fluid Dynamics (CFD) code used is ANSYS CFX. Before comparing the capability of the different turbulent models to predict unsteady behavior of cavitating flow along the hydrofoil, the study of the influence of the mesh resolution was performed in cavitating condition. This investigation was performed, on CLE hydrofoil, by monitoring the influence of for progressively finer meshes on the values of the drag C_D and lift C_L coefficients. Moreover, a study of the influence of the normal dimensionless distance to the wall (y+) was carried out on the hydrofoil surface. For the unsteady flow, a comparison of different turbulence models with the experiment leads to study the interaction of these models with the vapor pocket (detachment and collapse of vapor pocket). Two turbulence models were tested in this study: modified k-ε model and large eddy simulation (LES). In the present work, the predictions of velocity and pressure evolutions in the vicinity of the hydrofoil are compared to experimental data.

Keywords: Cavitation; CLE hydrofoil; URANS; LES.

NOMENCLATURE

C_D	drag coefficient
C_L	lift coefficient
C_μ	dimensionless constants
F_D	drag force
F_L	lift force
k	turbulent kinetic energy
i	angle of attack
L	characteristic length scale
$\dot{m}$	source term
$\dot{m}^+$	vaporization source term
$\dot{m}^-$	condensation source term
n_0	nuclei concentration per unit volume of pure liquid
P_∞	outlet pressure
P_v	vapor pressure
R	bubble radius
R_0	initial radius of bubble
S_M	momentum source
S	area of the hydrofoil
U	time averaged mixture velocity
U_t	parallel average velocities
U_∞	inlet flow velocity
u_τ	friction velocity
V_{vap}	volume of vapor in control cell
$y+$	normal dimensionless distance to the wall
α	vapor volume fraction
τ	surface tension
τ_ω	wall shear stress
γ	water volume fraction
μ	mixture viscosity
μ_l	vapor viscosity
μ_v	liquid viscosity
μ_t	eddy viscosity
ρ_l	liquid density
ρ_v	vapor viscosity
δ_{ij}	kronecker symbol

1. INTRODUCTION

When cavitation occurs in a hydraulic circuit, it can have adverse effects on industrial systems in question. The occurrence of the cavitation starts to reduce the performance of the machine (Dupont, 1993). It is increasingly accepted that the cavitation pocket at the leading edge constitutes the most erosive conditions (Avellan and Farhat, 1988, Bourdon *et al.* 1990, ITTC 1999 and Simoneau *et al.* 1989).

Several experiments have been widely applied in order to study the cavitation. The exact mechanisms of cavitating flow with complex characteristics have been identified across multiple experiences (Reisman *et al.* 1998, Chen *et al*. 2010, Tomov *et al.* 2016, Stutz and Reboud, 1997 and Zhang *et al.* 2015).

The experimental study of flow around a hydrofoil profile showed that the occurrence of cavitation is strongly explained by the fluid flow at the leading edge of the hydrofoil (Kravtsova *et al.* 2014). Moreover, numerous studies have shown that the re-entrant jet is considered as the main mechanism responsible for the shedding of cavity (Arndt *et al.* 2000, Altimira and Fuchs, 2015, Dreyer *et al.* 2014, Decaix and Goncalvès, 2013, Goncalvès and Charrière, 2014, Roohi *et al.* 2013, Zhang *et al.* 2014 and Yu *et al.* 2014).

The different mathematical formulations of the cavitating flows can be classified into two groups: two separated fluids model and homogenous mixed model.

By using a homogenous mixture model for the modeling of the cavitating turbulent flow, the system needs two closures: a closure for eddy viscosity and a closure for vapor volume fraction. Two closures techniques of the fraction volume are suggested. Either, the transport equation with the source terms (TEM) (Kunz *et al.* 2000, Singhal *et al.* 2002, Senocak and Shyy, 2002 and Zwart *et al.* 2004) or the state equation (EOS) (Delgosha *et al.* 2003, Barre *et al.* 2009 and Mostafa *et al.* 2015). However, the TEM model offers the possibility to modelise the interaction between the two phases by means of a source terms through minimizing the empirical aspects. Thus, we opt for adopting the transport equation in this study. We can cite the works which adopted the same procedure based on the formulation of the homogenous mixture (Sauer and Schnerr, 2000, Yuan *et al.* 2001 and Ait Bouzia, 2006, Ahuja *et al.* 2001, Chen and Heister, 1995, Schmidht *et al.* 1997 and Shnerr and Sauer, 2001).

In cavitating flow simulations, the turbulence model (Guerri *et al.* 2015) is necessary because the cavitation is fundamentally unsteady in nature and there are interactions between the boundary layer during cavity development and the cavity interface. Whereas the current Reynolds average Navier–Stokes (RANS) equation approach (Khlifi and Lili 2011) has been broadly used to model turbulent flows in manufacturing, the RANS models with eddy viscosity turbulence models have limited ability to simulate unsteady cavitating turbulent flows and need some modifications (Chen and Lu, 2008; Coutier-Delgosha *et al.,* 2003; Decaix and Goncalves, 2013; Goncalves, 2011; Huang *et al.,* 2013). Furthermore there have been attempts to predict the unsteady cavitating flow using LES (Aghaee-shalmani and Hakimzadeh, 2015). LES for cavitating flows are expected to give better accuray and predictions of larger-scale turbulent eddies (Bensow and Bark, 2010; Dittakavi *et al.,* 2010; Luo *et al.,* 2012; Roohi *et al.,* 2013).

The objective of this paper is to study the effect of cavity growth and shedding on the dynamics of vortical flows by analyzing unsteady cavitating flows around a CLE hydrofoil. This paper is organized as follows. Mathematical formulations and numerical method of the CFD including the cavitation model are described in section in section 2. The investigation of mesh and y+ influence is presented in section3. Detailed results and discussions are then given in section 4 and the conclusion in section 5.

2. MATHEMATICAL MODEL

2.1 Governing Equations

In ANSYS-CFX, the hydrodynamic equations for a homogeneous mixture flow are written respectively by Eqs. (1), (2) and (3):

$$\nabla U = \dot{m}\left(\frac{1}{\rho_l} - \frac{1}{\rho_v}\right) \tag{1}$$

$$\frac{\partial \rho}{\partial t} + \nabla.\left(\rho U U\right) = -\nabla P + \nabla.\tau + S_M \tag{2}$$

$$\frac{\partial \gamma}{\partial t} + \nabla.\left(\gamma U\right) = \frac{\dot{m}}{\rho_l} \tag{3}$$

The above equations consists of the continuity equation, the momentum equation, for vapor-liquid mixture considered homogeneous and incompressible and the volume fraction equation for the liquid phase, respectively, where ṁ represents the inter-phase mass transfer rate due to cavitation, P the time averaged pressure, U represents the time averaged mixture velocity, ρ_l the liquid density, ρ_v the vapor density, S_M are momentum sources, τ is stress tensor. The vapor volume fraction α and the water volume fraction γ are defined as follows:

$$\alpha = \frac{Volume\ of\ vapor}{Total\ volume} \quad \gamma = \frac{Volume\ of\ liquid}{Total\ volume} \tag{4}$$

The vapor volume fraction is related to liquid volume fraction as:

$$\alpha + \gamma = 1 \tag{5}$$

Finally the effective density ρ and the dynamic viscosity μ of the vapor-water mixture are given by Eqs. (6) and (7), respectively:

$$\rho = \rho_v \alpha + (1 - \alpha)\rho_l \tag{6}$$

$$\mu = \mu_v \alpha + (1-\alpha)\mu_l \tag{7}$$

2.2 Cavitation Model

The transition from one phase to another is ensured by the inter-phase transfer via source terms in the transport equation. This method has the advantage to take into account the time dependence of mass transfer phenomena by empirical laws in the source terms. In this study, we applied the cavitation model of Kanfoudi and Zgolli (2011).

This model is devoted to the development of source term for the transport equation to modeling the cavitating turbulent flow which takes account of the interfacial velocity of bubble at collapse. It is based on the Rayleigh–Plesset equation, which emphasizes the fundamental bubble dynamics.

The velocity of collapse is written by:

$$\dot{R} = \frac{dR}{dt} = -\sqrt{(\frac{2}{3}\frac{P - P_v}{\rho_l})(\frac{R_0^3}{R^3} - 1)} \tag{8}$$

Where R is the bubble radius and R_0 is the initial radius of bubble.

The vapor volume fraction can be written as:

$$\alpha = \frac{V_{vap}}{V_{tot}} = \frac{n_0 (4/3)\pi R^3}{1 + n_0 (4/3)\pi R^3} \tag{9}$$

Where n_0 is defined as nuclei concentration per unit volume of pure liquid ($n_0 \approx 10^{12}$ nuclei/m^3 for water (Fujimoto *et al.* 1994)) and R is the bubble radius.

The source term of this model can be written by the Eq. (10)

$$\dot{m} = C.f_\alpha \sqrt{|g(\alpha, p)|}.sign\left[g(\alpha, p)\right] \tag{10}$$

$$\text{With} C = \sqrt{6}\sqrt[3]{\frac{4}{3}n_0\pi}\frac{\rho_v \rho_l}{\rho} \tag{11}$$

$$f_\alpha = \alpha^{\frac{2}{3}}(1-\alpha)^{\frac{4}{3}} \tag{12}$$

$$g(\alpha, p) = \left[\frac{P_v - P}{\rho_l}\right](1 - \phi(\alpha)) \tag{13}$$

$$\phi(\alpha) = \frac{4R_0^3 n_0 (1-\alpha)}{\alpha} \tag{14}$$

Finally, the specific mass transfer rate is defined as:

$$\dot{m} = \begin{cases} \dot{m}^+ = \sqrt{6}\sqrt[3]{\frac{4}{3}n_0\pi}\frac{\rho_v \rho_l}{\rho}\alpha^{\frac{2}{3}}(1-\alpha)^{\frac{4}{3}}\sqrt{\left[\frac{P_v - P}{\rho_l}\right](1-\phi(\alpha))} \\ \dot{m}^- = \sqrt{6}\sqrt[3]{\frac{4}{3}n_0\pi}\frac{\rho_v \rho_l}{\rho}\alpha^{\frac{2}{3}}(1-\alpha)^{\frac{4}{3}}\sqrt{\left[\frac{P - P_v}{\rho_l}\right](1-\phi(\alpha))} \end{cases} \tag{15}$$

For more details, you can see Kanfoudi and Zgolli (2011).

2.3 Turbulence Model

The first order-closures are the preferred means to approach the Reynolds tensor. The approximation in the turbulence modeling suggests that the Reynolds tensors are assumed to be proportional to the average speed gradients.

$$-\overline{u_i u_j} = \mu_t \left(\frac{\partial U_i}{\partial x_j} + \frac{\partial U_j}{\partial x_i}\right) - \frac{2}{3}k\,\delta_{ij} \tag{16}$$

Where μ_t is the eddy viscosity and δ_{ij} the Kronecker symbol and k is the average turbulent kinetic energy per unit of given mass.

Based on semi-empirical equations, the k-ε standard model (Jones *et al.* 1999 and Launer and Spalding, 1974) has two equations, one for the turbulent kinetic energy (k) and the other for its viscous dissipation rate (ε). With the analogy of Prandtl-Kolmogorov, the eddy viscosity is given by:

$$\mu_t = C_\mu \frac{k^2}{\varepsilon} \tag{17}$$

Where C_μ is a dimensionless constant.

A simple modification of the k-ε model, initially proposed by Reboud *et al* (1998) was applied directly in the expression of the eddy viscosity by writing it:

$$\mu_t = f(\rho) C_\mu \frac{k^2}{\varepsilon} \tag{18}$$

$$C_\mu = 0.09 \tag{19}$$

$$f(\rho) = \rho_v + \alpha^n (\rho_l - \rho_v) \quad \text{with } n = 10 \tag{20}$$

The advantage of the modified k-ε model compared to the standard k-ε model in unsteady state is that it captures the detachment of the vapor pocket.

3. SIMULATION SETUP

The unsteady cavitating flow simulations were started from a steady cavitating flow field. The cavitation model and unsteady solver were then turned on for cavitating flow simulation. The time step was set to 4.46×10-5 s because Tref=L/U∞ =8.92 ×10-3 s and Tref/200=4.46×10-5 s (T_{ref}/200, where T_{ref}=L/U_∞ and U_∞ is the inlet flow velocity) (Coutier-Delgosha *et al.*, 2003).

Before starting the simulations, four steps are adopted. The first step is to prepare the geometry, the next step is meshing the geometry of each blocks, third stage gives the boundary conditions the last step is to start the simulation and observe the results.

A CLE hydrofoil was used in the present study. The experiments of the unsteady cavitating flow behavior around a CLE hydrofoil were realized in a cavitation tunnel by Dular *et al.* (2009).

3.1 Geometry

The dimensions of the hydrofoil are presented by the Fig. 1:

In the case of this application, the computational

domain is divided into 8 blocks with a structured grid, as shown in the Fig. 2. The hydrofoil is placed in a cavitation tunnel at an angle of 5°.

Fig. 1. Dimension of a CLE hydrofoil.

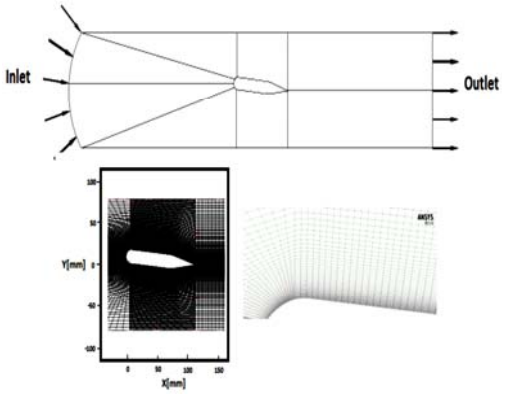

Fig. 2. CLE hydrofoil domain gird, *i*= 5°, y+=30, C-gird structure, with 8 blocks.

3.2 Boundary Conditions

The solutions of the governing equations are calculated in a given geometric configuration by combining the conditions for specific limits (velocity, pressure).

1. The input condition (Inlet): The input velocity U_∞ is steadily fixed to the entire border to generate a flow which is established more quickly, U_∞=13 m/s.
2. The output condition (Outlet): We chose in our calculations to fix the value of the static pressure at a constant value over the entire border P_∞, calculate as a function of the value of σ.
3. The friction condition to solid walls (Wall): It allows modelling the adhesion between the fluid and the solid wall. Normal speed to the solid wall is imposed zero and the tangential velocity is considered equal to the speed of the wall (zero in this case).
4. The condition of symmetry (Symmetry): It allows modeling the case where a flow of a side of the symmetry plane is the mirror image of the flow on the other side of the symmetry plane.

The following Table 1 contains the data used as boundary conditions for the hydrodynamic validation.

The cavitation number σ which was presented by Knapp *et al.* (1970). It measures the sensitivity of the flow to the pressure variation, expressed by the Eq. (21):

$$\sigma = \frac{P_\infty - P_v}{\frac{1}{2}\rho_l U_\infty^2} \tag{21}$$

The Reynolds number can be express by:

$$R_e = \frac{U_\infty . L}{\upsilon} \tag{22}$$

In our case L is chord of hydrofoil which is taken 0.116 m. With U_∞ = 13 m/s is a characteristic velocity of the flow and ν is a kinematic viscosity (m^2/s). The Reynolds number is 1.5×10^6, we can conclude that the flow is turbulent which justifies the choice of the turbulent model.

3.3 Mesh Independence

To verify the independence of numerical solution from the mesh quality, a study of mesh influence was realized by controlling the drag and lift coefficients, which were written as follows:

$$C_D = \frac{F_D}{\frac{1}{2}\rho U_\infty^2 S} \; ; \; C_L = \frac{F_L}{\frac{1}{2}\rho U_\infty^2 S} \tag{23}$$

With S is the projected area of profile, F_D and F_L are the drag and lift forces around the hydrofoil.

A modification of the mesh involves significant changes of the results. The influence of the mesh is not only in terms of nodes, but also in terms of the quality of the mesh, especially at the leading edge. We therefore speak of the distance of the first mesh.

In this study we tested four configurations that are shown in Table 2.

Table 1 Numerical values of boundary conditions

Constant	Symbol	Value
Reference velocity	U_∞	13 m/s
Static pressure at the outlet	calculate as a function of the value of σ	
Length of chord	L	0.116 m
Saturation pressure	P_V	3200 Pa
Cavitation number	σ	2
Liquid density	ρ_l	997 kg/m^3

Table 2 Results of the mesh independence test

	Numb-er of cells	*number of nodes*	C_D	C_L
M1	29 808	61 600	0.1140	0.6962
M2	37 128	76 500	0.1262	0.6715
M3	48 708	100 000	0.1265	0.6693
M4	57 309	118 056	0.1266	0.6692

The more we have a variation of the mesh, the more

the calculation of the drag and lift coefficients are affected.

From the results shown in Table 2, it is indicated that the differences between the M3 and M4 can be neglected, thus the M3 was selected as the final structured mesh.

3.4 Influence of Y+

y+ is the normal dimensionless distance to the wall. The values of y+, for the k-ε turbulence model vary between $30 \leq y^+ \leq 300$. In fact, we search to model the transition zone between laminar and turbulent boundary layer. In the logarithmic area, the velocity profile is given by the following equation:

$$u^+ = \frac{U_t}{u_\tau} = \frac{1}{k}\ln\left(y^+\right) + C \tag{24}$$

$$\text{Where } y^+ = \frac{\rho \Delta y u_\tau}{\mu} \tag{25}$$

$$u_\tau = \left(\frac{\tau_\omega}{\rho}\right)^{1/2} \tag{26}$$

u_τ is the friction velocity, U_t is the parallel average velocity to the wall with a distance equals a Δy from the wall, k is the von Karman constant, τ_ω is the wall shear stress and C is an empirical constant related to the thickness of the viscous sub-layer.

In the wall formulations, two definitions of Δy are available in Solver Yplus and Yplus. In the post processor, the definition for the Yplus is given by the standard formulation of y^+ used in CFD.

$$y^+ = \frac{\sqrt{\tau_\omega / \rho}.\Delta n}{\nu} \tag{27}$$

Where Δ*n* represents the distance between the two first consecutive points off the wall.

CFX-Solver uses the Yplus variable, which adopts several formulations to define the distance of the first point from the wall. This allows having optimum results in terms of robustness and accuracy.

The definition of scalable wall function y^+ is:

$$y^+ = \max\left(y^*, 11.06\right); \; y^* = \frac{u^* \Delta n / 4}{\nu} \tag{28}$$

We performed a series of four test values of y^+ to examine the solution sensitivity of Yplus and Yplus solver.

Table 3 recapitulates the different results of y^+. to have an optimal solution, it is necessary that the Yplus value reach the Yplus Solver. Thus, according to the results shown in Table 4, we can choose $y^+ = 60$ as a normal dimension distance from the wall.

The mesh is taken fine enough to capture the viscous effects of the boundary layer close to the wall of the hydrofoil ($y^+ \approx 1$) for the calculation based on the formulation of LES.

The machine used for these simulations is a PC with a microprocessor (Intel Pentium 2117U), a clock frequency of 1.8 GHz and 4 GB of random access memory (RAM).

Table 3 Numerical values of initial conditions

Y+	Y plus	Y plus solver
30	3.682	11.07
40	2.6	11.13
50	7.77	11.12
60	11.63	11.64

Table 4 Computing time for LES and modified K-ε

	k-ε modified	LES
Time steps (s)	10^{-5}	10^{-5}
Simulation time (s)	0.5	0.5
Max courant number	5	5
Computing time CPU (days)	18	26

4. RESULTS AND DISCUSSIONS

The sheet cavitation is frequently observed on hydrofoils. It generally appears in the vicinity of the leading edge. In some cases, the partial cavitation per pocket is unstable and may cause significant damage. This type of flow is highly unsteady at the vapor pocket closure zone. However, early in its development, the closure is well localized in space, and the pocket is often stable. During the development of the cavity, the spatial variations of the closing appear, and under certain conditions the pocket is destabilized and implodes violently. In this operating regime, the volume of the vapor cavity oscillates between a minimum and a maximum. The destabilization process leads to the emission of vortex and biphasic structures, called cavitation cloud, known to generate a high overpressures and to be highly erosive.

We consider the case of a 2D CLE hydrofoil. The angle of incidence of the profile $i = 5°$, a cavitation number $\sigma = 2$. The domain is composed of one single row of meshes in the transverse direction (1 x 100 000 cells) with symmetry conditions on its border, at the entrance a velocity $U_\infty = 13$ m/s, turbulent intensity is 1%, the turbulent length scale is equal to 0.001 m. The output is set to the average static pressure which is defined by the number of cavitation. The top and bottom walls are modeled with the slip conditions. The walls of the hydrofoil are modeled as nonslip. Simulations are performed using a scheme of second order for the continuity and momentum equations.

For transport equations of the volume fraction of vapor and the turbulent equations, we used a hybrid

scheme of the second order. A comparative with a numerical model will be presented for confrontation and validation of the proposed model. The two turbulence models employed in this study are: LES (Shirani *et al.* 2011) and the modified k-ε model.

We present in Fig. 3 experimental visualizations of CLE hydrofoil profile, of cavitating flow in unsteady state. The main vapor pocket located at the leading edge is very unstable with an almost cyclically pocket detachment. These small pockets are convected away from the area of their birth, leading edge to the trailing edge where the pressure is high thus causing their implosion. Soon as the length of the main vapor pocket reaches a maximum value, depending on the cavitation number and the angle of incidence, a re-entrant jet occurs. It moves below the main vapor pocket breaking it into small pockets.

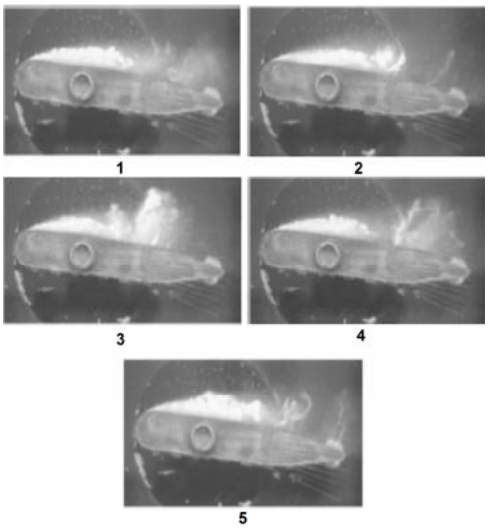

Fig. 3. Instantaneous visualization of the cavitating flow around the CLE hydrofoil profile, i=5°, σ=2, U∞=13m/s Dular and Delgosha (2009).

Numerically, for this case, we conducted a comparative study of two turbulence models: LES and modified k-ε.

The mesh is taken fine to capture the viscous effects of the boundary layer near the wall of the hydrofoil. The steady state solution is used as an initial condition for unsteady Reynolds average Navier–Stokes (URANS) and LES calculations. The conventional turbulence models based on two equations in the homogeneous mixture formulation are failing to calculate the typical case of cavitation. The reason for this failure is that the values of the turbulent viscosity are artificial.

4.1 Vapor pocket Visualization

The volume of vapor is an excellent variable to identify the periodicity of the training cycle and collapse of the vapor pocket. We can perfectly distinguish from Fig. 4 a peak which presents the maximum steam production for both cases.

The volume of vapor in dimensionless form given by the following expression:

$$V_{vap,2D} = \frac{1}{c^2}\sum_{i=1}^{N} \alpha_i V_i \tag{29}$$

With N number of nodes in the mesh, α_i is the volume fraction of vapor and V_i is the volume of fluid.

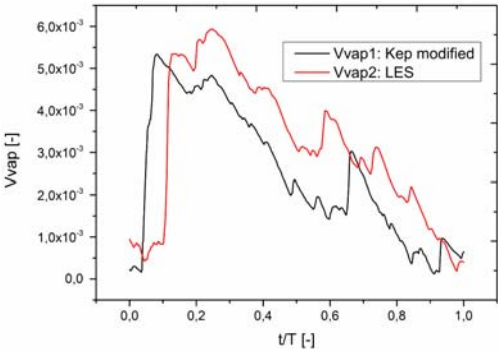

Fig. 4. Comparison of the vapor volume of the URANS and LES model for a cycle of a vapor pocket.

The vaporization process is characterized by the acceleration towards a maximum steam production. For against, the collapse process is very slow, which is due to small steam cavities convected by the flow that takes a long time to collapse.

The measure of CPU time and numerical setup is shown in Table 4.

Numerical simulations are qualitatively very similar to the experimental observations. It can be concluded that the behavior of LES is similar to modified k-ε model. There is just an underestimation of the pocket volume, which may be explained by the empirical formulation of the employed density. However the URANS model allows to save more than 30% of computing time compared to LES in Table 4 and to avoid the refinement of the mesh.

The Fig. 5 and Fig. 6 report a typical cycle of the cavitation pocket of the proposed model respectively for modified k-ε model and LES.

The vapor pocket is localized at the leading edge of the hydrofoil, with a considerable thickness. For a period of formation and collapse of the vapor pocket, we can see two processes highlighted by the calculated vapor volume. If we take the case of LES as reference. We observe the convected vapor cavities by the flow resulting from the previous cycle (0.1T). Then we observe a new vapor pocket which expands at the leading edge called that is the growth phase (0.2T to 0.5T). It reaches its maximum length at 0.5T. As the re-entrant jet reaches the region of strong pressure gradient (the pocket closed area), it becomes more important and starts moving upstream toward the leading edge along the surface of the hydrofoil below the vapor pocket (0.6T to T). It decomposes the main vapor pocket in small cavities that are then taken by the flow downstream (trailing edge) and a new cycle is born.

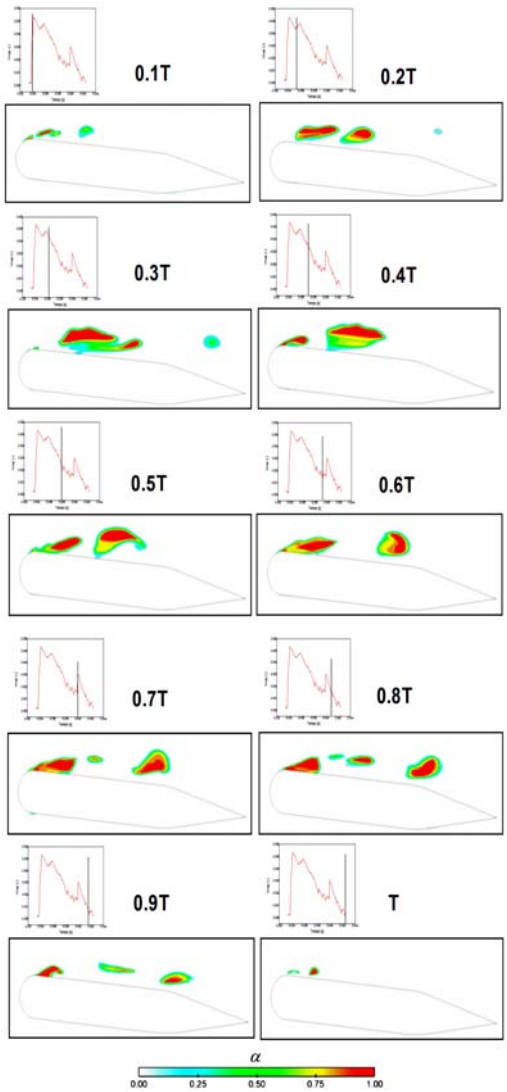

Fig. 5. Presentation of the volume fraction of vapor; σ=2, i=5°, turbulence model (modified k-ε) for one cycle T=0.01s.

4.2 Velocity distribution validation

In this section, a comparison between the time-averaged numerical and experimental velocity profiles is presented in Fig 8 and Fig 9. Experimental results are obtained from particle image velocimetry (PIV) experiments, while numerical results are calculated by time averaging the results saved between the time of appearance and disappearance of cavitation pocket.

Two velocity components have been studied in this section. The first is the component u (horizontal direction) and the second is the component v (vertical direction). The component u is investigated at five positions above the hydrofoil.

The simulation results are a good agreement with experimental data. As we progress towards the surface of the hydrofoil, the flow velocity starts to decrease (the transition usually occurs roughly at the boundary of the sheet cavity). For position x = 0mm (leading edge) and x =64mm (downstream from the sheet cavity), no re-entrant jet is detected. On the other side at stations x =16, 32, and 48 mm, a reverse flow is plainly observed both in numerical and experimental results. The extension and magnitude of the re-entrant jet are properly predicted by the two models, while its thickness is slightly overestimated by the URANS model (see planes x =16, 32 and 48 mm).

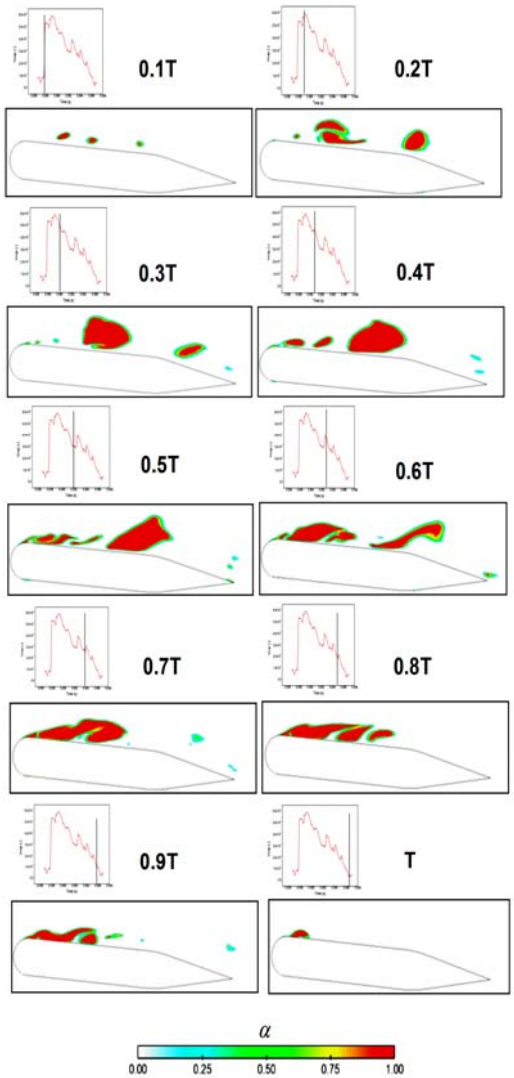

Fig. 6. Presentation of the volume fraction of vapor; σ=2, i=5°, LES, for one cycle T=0.01s.

Figure 8 shows the velocity component v (vertical direction). Velocities were measured and predicted on four different planes above the hydrofoil. At the leading edge of the hydrofoil, the velocity component v has undergone a significant increase. This growth is more remarkable in the vicinity of the hydrofoil (plane y=0 mm). The maximum velocity of the v component is attained at the point of transition from the plane surface of the hydrofoil (x =20 mm) to the circular leading edge.

The velocity component has undergone a significant decrease throughout the x direction, from the different planes y = 0, 5, 10 and 15 mm. We notes it reaches a slightly negative value in the aft part of

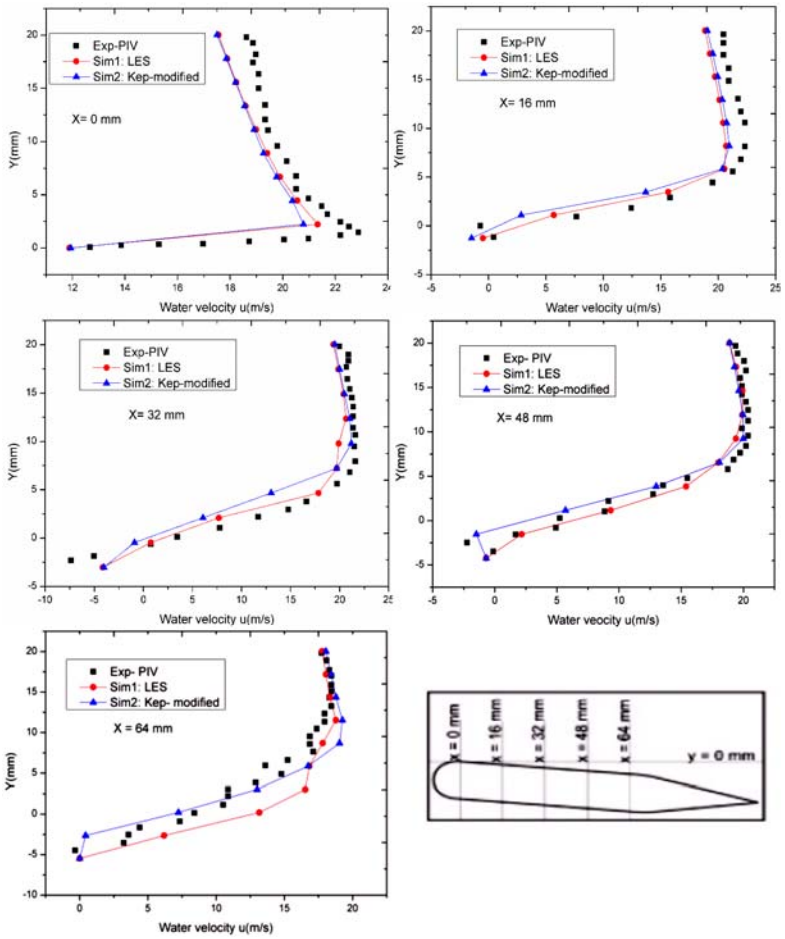

Fig. 7. Comparison between experimental and numerical simulation of velocity profile in the x direction at the positions x=0; 16; 32; 48 and 64 mm (Exp. data from Dular and Delgosha (2009)).

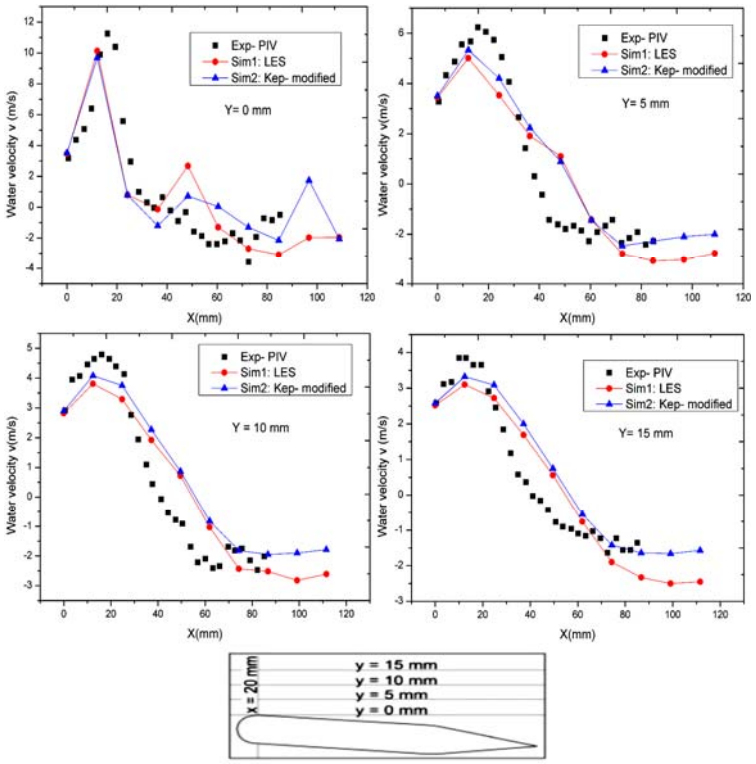

Fig. 8. Comparison between experimental and numerical simulations of averaged-time velocity profile (vertical direction) on four planes y=0; 5; 10 and 15 mm (Exp. data from Dular and Delgosha (2009)).

the hydrofoil, and this can be explained by the angle of attack of 5°. This decrease was adequately predicted by the two models proposed.

We note that the simulation with LES approaches the experimental measurements compared to URANS. This is quite normal since LES can capture the velocity fluctuations.

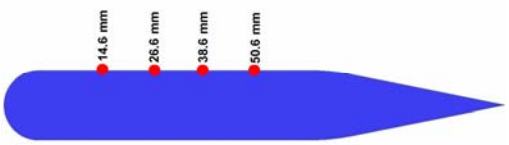

Fig. 9. Location of the pressure sensors.

However, the cycle of evolution of the vapor pocket shows that URANS model allows reproducing it better than LES. This leads us to conclude that URANS model is able to predict the detachment mechanisms of cavitation pocket formation better than LES. In addition, it makes the computational cost lower than LES which requires more computing resources.

4.3 Pressure Oscillations Validation

We propose in what follows a confrontation between the numerical results and the experimental data of pressure variation.

The pressure sensor positions are shown in Fig. 9 The modified k-ε and LES were adopted as turbulence model in this comparison.
The experimental pressure oscillations were available solely for the following conditions σ = 2.7 and v = 16 m/s.

Once cavity shedding happens, the pressure oscillations along the hydrofoil surface vary greatly due to the dynamic behavior of cavitation. Numerical predictions of pressure fluctuations at four positions X=14.6, 26.6, 36.6.and 50.6 mm are shown in Fig. 10 along with the experimental data (Dular and Delgosha 2009). Concerning the sensor placed at X= 14.6 mm, we observe that the pressure is nearly constant with a slight fluctuation of some mbar. This is explained by the fact that the sensor is placed on the area where the pocket remains stable. The cavitation cloud detachments and collapses caused by the re-entrant jet are performed at X= 26.6 and X=36.6 mm. All this explains the large variation of pressure that reaches 14 bars for a short period of time. The pressure oscillations predicted by URANS model at X= 26.6 mm are slightly different from that of experimental data. One possible cause of this disagreement is due to the fact that cavitation inception and evolution from the leading edge is started by the stream-wise vortex which is not resolved by present model.

The curve obtained at X=50.6 mm shows a decrease in the pressure amplitude, and this is due to the position of the sensor which is a non-cavitation area. Generally, the pressure oscillations are very well predicted in terms of amplitude at all positions.

Numerically, the URANS and LES models approach the experimental data. URANS presents significant fluctuations due to the fact it does not perfectly captures the flow structure in addition with LES.

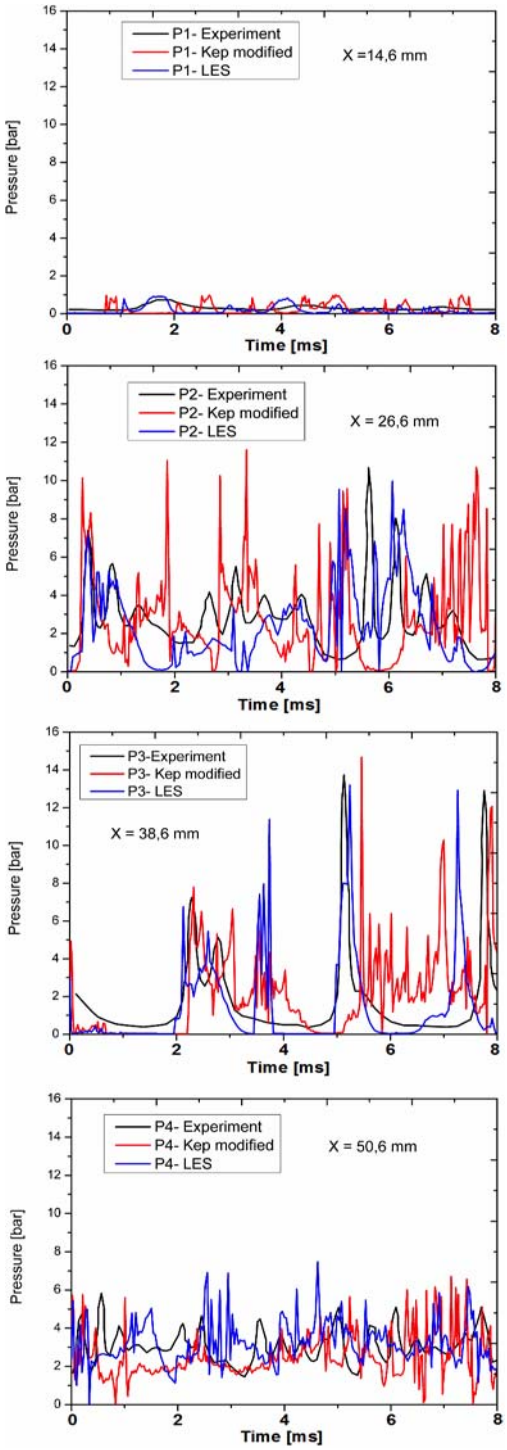

Fig. 10. Experimental and pridected pressure oscillations (Exp. data from Dular and Delgosha (2009)).

An increase in pressure oscillations cannot cause erosion by itself, but it can carry enough energy to give birth to other events.

The process of pit formation is very intricate. The theory presented by (Dular and Delgosha 2009 and

Dular *et al*. 2006) explains the pit formation in the following way: The cavitation cloud moves with the flow and collapses in a higher pressure zone. The shock wave issued at the collapse of the cavitation cloud collapse attains a magnitude of up to several MPa and influences the bubbles that are placed near the wall. A sufficient magnitude of pressure wave can act on the bubbles of a spherical shape that are placed close to the surface of the submerged body. The form of the bubble becomes unstable, and begins to oscillate. If the amplitude of pressure oscillations is high enough, a micro-jet phenomenon can occur. The fluid that surrounds the bubble takes a form of jet through the bubble in the direction towards the structure surface. This micro-jet can reach high local velocities that provoke a shock (the order of magnitude is bigger than 1GPa, the duration is roughly 1 ns and the affected zone is in order of a few μm^2) with high local tension of the material. The damage of the solid surface appears in a form of pits.

5. CONCLUSION

This study is a contribution to physical modeling and numerical simulation which were performed on a CLE hydrofoil at angle of attack of 5° of unsteady cavitating flow. Numerical study of the unsteady cavitating turbulent flow was carried out by means of a Large Eddy Simulation (LES) and URANS model coupled with a homogeneous cavitation model. This investigation is based on a Kanfoudi model. This model is based on a homogeneous mixture approach in which the transition from one phase to another is ensured through the interphasic transfer using the source terms. The study of mesh influence was performed by monitoring the drag and lift coefficients. The choice of y+ is based on a sensitivity analysis of Yplus vis-à-vis Yplus solver. The predicted cavitation shedding dynamics behavior, such as the cavity growth, the detachment and the collapse downstream, agrees fairly well with the experimental observations. However, the modified k-ε model and LES were used for simulation of unsteady cavitating flow because. The instantaneous pressure oscillations and vapor volume fraction computed are shown at different time steps. The numerically predicted velocity profiles present a good agreement with experimental data. Pressure fluctuations along the CLE hydrofoil surface, which are excited by periodic cavitation shedding dynamics, was simulated and confronted with the available experimental data. The results showed that the LES simulation can reasonably predict pressure oscillations on the suction surface of the hydrofoil, except for the trailing edge are overestimated.

The obtained results verify the relationship between the pressure oscillations and the cavity shedding process and demonstrate that the cavity volume acceleration is the principal source of the pressure fluctuations around the hydrofoil. These results are necessary for the understanding the mechanism of the cavitation excited pressure pulsations, which will help evolution of engineering designs to control these oscillations.

REFERENCES

Aghaee-Shalmani, Y. and H. Hakimzadeh. (2016). Numerical modeling of 2-D and 3-D flows using artificial compressibility method and collocation mesh. *Journal of Applied Fluid Mecanics* 9(5), 2333-2345.

Ahuja, V., A. Hosangadi and S. Arunajatesan (2001). Simulations of caviting flows using hybrid unstructured meshes. *J. Fluids Engng*. 123, 331-339.

Altimira, M. and L. Fuchs (2015). Numerical investigation of throttle flow under cavitating conditions. *International Journal of Multiphase Flow* 75, 124-136.

Arndt, R. E., C. Song, M. Kjeldsen, J. He and A. Keller (2000). Instability of partial cavitation: a numerical/experimental approach. In *Proceedings of the Twenty-Third Symposium on Naval Hydrodynamics, Val de Reuil, France.*

Avellan F. and M. Farhat M (1988) Supression Générée par un Tourbillon cavitant La Houille Blanche. - 527-533.

Barre, S., J. Rolland, G. Boitel, E. Goncalves and R. F. Patella (2009). Experiments and modeling of cavitating flows in venturi: attached sheet cavitation. *European Journal of Mechanics B/Fluids* 28, 444-464.

Bensow, R.E., Bark, G., (2010). Implicit LES Predictions of the Cavitating Flow on a Propeller. J. Fluids Eng. 132(4), 041302.

Bourdon P. et al. (1990) Vibratory caracteristics of erosive cavitation vortices downstream of a fixed leading caviy, Belgrade, Yugolslavia

Bouziad, Y. A. (2006). physical modelling of leading edge cavitation : computational methodologies and application to hydraulic machinery, EPFL, Lausanne,Suisse.

Chen, C., C. Nicolet, K. Yonezawa, M. Farhat, F. Avellan, K. Miyagawa and Y. Tsujimoto (2010). Experimental study and numerical simulation of cavity oscillation in a conical diffuser. *International Journal of Fluid Machinery and Systems* 3, 91-101.

Chen, Y. and C. J. Lu (2008). A Homogenous-Equilibrium-Model Based Numerical Code for Cavitation Flows and Evaluation by Computation Cases. *J. Hydrodyn.* 20, 186-194.

Chen, Y. and S. D Heister. Two-phase modelling of cavitated flows (1995). In *ASME Cavitation and Multiphase Forum*, 24, 799-806.

Coutier-Delgosha, O., R. Fortes-Patella, J. L. Reboud, M. Hofmann and B. Stoffel (2003). Experimental and numerical studies in a centrifugal pump with two-dimensionalcurved blades in cavitating condition. *Journal of Fluids Engineering* 125(6), 970-978.

Decaix, J. and E. Goncalvès (2013). Compressible

effects modeling in turbulent cavitating flows. *European Journal of Mechanics - B/Fluids* 39, 11-31.

Dittakavi, N., A. Chunekar and S. Frankel (2010). Large eddy simulation of turbulent-cavitation interactions in a venturi nozzle. J. Fluids Eng. 132(12), 121301.

Dreyer, M., J. Decaix, C. Münch-Alligné and M. Farhat (2014). Mind the gap: a new insight into the tip leakage vortex using stereo-PIV. *Experiments in Fluids* 55(11), 1-13.

Dular, .M and O. Coutier-Delgosha (2009). Numerical modelling of cavitation erosion. *International Journal For Numerical Methods In Fluids* 61(12), 1388-1410.

Dular, M., B. Stoffet and B. Sirok (2006). Development of a cavitation erosion model. *Wear* 261, 642–655

Dupont, PH (1993). Etude de la dynamique d'une poche de cavitation partielle en vue de la prediction de l'érosion dans les turbomachines hydrauliques. thèse de doctorat. EPFL, Suisse.

Fujimoto, H. G., T. NishikoriI T. Hojyo Y., Tzumakoto T.,Senda J (1194). Modelling of atomization and vaporization process in flash boiling spray, France.

Goncalves, E. (2011). Numerical Study of Unsteady Turbulent Cavitating Flows. *Eur. J. Mech. B-Fluid* 30, 26-40.

Goncalvès, E. and B. Charrière (2014). Modelling for isothermal cavitation with a four-equation model. *International Journal of Multiphase Flow* 59, 54-72.

Guerri, O., E. Liberge and A. Hamdouni (2016). Numerical simulation of the turbulent flow around an Oval-sail. *Journal of Applied Fluid Mechanics* 9(4), 2009-2023.

Huang, B., Y. L. Young, G. Y. Wang, W. Shyy (2013). Combined experimental and computational investigation of unsteady structure of sheet/cloud cavitation. *J. Fluids Eng.* 135, 071301.

ITTC (1999). Final report of the Specialist Committee on Computational Method for Propeller Cavitation [Rapport]. - [s.l.] : In Proceedings of 22 nd International Towing Tank Conference.

Jones S., Evans G. et Galvin K. Bubble nucleation from gas cavities a review [Article] // Advances in Colloid and Interface Science 80. - 1999. - 27-50.

Kanfoudi, H. and R. A. Zgolli (2011). Numerical model to simulate the cavitating flows. *International Journal of Modeling, Simulation, and Scientific Computing* 2(03), 277-297.

Khlifi H. and T. Lili (2011). A Reynolds stress closure for compressible turbulent flow. *Journal of Applied Fluid Mecanics.* 4(2), 99-104.

Knapp, R. T., J. W. Daily and F. G. Hammitt (1970). Cavitation. Engineering Societies Mono-graphs, New York.

Kravtsova, A. Y., D. M. Markovich, K. S. Pervunin, M. V. Timoshevskiy and K. Hanjalić (2014). High-speed visualization and PIV measurements of cavitating flows around a semi circular leading-edge flat plate and NACA0015 hydrofoil. *International Journal of Multiphase Flow* 60, 119-134.

Kunz, R. F., D. A. Boger and D. R. Stinebring (2000). A preconditioned Navier-Stokes method for two-phase flows with application to cavitation prediction. *Computer and Fluids* 29, 849-875.

Launder, B. E. and D. B. Spalding (1974). The numerical computation of turbulent flows Comp Meth Appl Mech Eng 3(2), 269-289.

Luo, X. W., B. Ji, X. X. Peng, H. Y. Xu and M. Nishi (2012). Numerical simulation of cavity shedding from a three-dimensional twisted hydrofoil and induced pressure fluctuation by large-eddy simulation. *J. Fluids Eng.* 134(4).

Mostafa, N, M. M. Karim and M. M. A. Sarker (2016). Numerical prediction of unsteady behavior of cavitating flowon hydrofoil using bubble dynamics cavitation model. *Journal of Applied Fluid Mecanics* 9(4), 1829-1837.

Reboud, J. L., B. Stutz, O. Coutier (1998). Two phase flow structure of cavitation: Experiment and modeling of unsteady effects. 3rd Int. Symp. on Cavitation, 39-44, Grenoble, France.

Reisman, G., Y. C. Wang, C. Brennen (1998). Observations of shock waves in cloud cavitation. *Journal of Fluid Mechanics* 355, 255-283.

Roohi, E., A. P. Zahiri and M. Passandideh-Fard (2013). Numerical Simulation of Cavitation around a Two-Dimensional Hydrofoil Using VOF Method and LES Turbulence Model. *Applied Mathematical Modelling* 37, 6469-6488.

Sauer J. and G. H. Schnerr (2000). Unsteady cavitating flow-A new cavitation model based on a modified front capturing method and bubble dynamics, ASME, Fluid Engineering Summer Conference, 11-15, Boston, MA.

Schmidt, D. P., C. J. Rutland and M. L. Corradini (1997). A numerical study of cavitating flow through various nozzle shapes, SAE paper 971597.

Schnerr, J. and G. H. Sauer (2001). Physical and numerical modeling of unsteady cavitation dynamics, In Proceedings of the 4th International Conference on Multiphase Flow (IMCF-01). - New Orleand, USA.

Senocak I and W. Shyy (2002). Evaluation of cavitation models for navier-stokes computations, In Proceedings of ASME

FEDSM.

Shirani, E., F. Ghadiri and A. Ahmadi (2011). Modeling and simulation of interfacial turbulent flows. *Journal of Applied Fluid Mecanics.* 4(2),. 43-49,

Simoneau, R., F. Avellan and Y. Kuhn de chizelle (1989). On line measurement of cavitation erosion rate on a 2D NACA profile, Proc. of Int Symposium on cavitation noise and erosion in fluid systems, ASME, 95-102, San Francisco, US

Singhal, A. K., M. M. Athavale, H. Li and Y. Jiang (2002). Mathematical basis and validation of the full cavitation model. *Journal of fluids engineering* 124(3), 617-624.

Stutz, B., J. L. Reboud (1997). Two-phase flow structure of sheet cavitation. Physics of Fluids 9, 3678-3686.

Tomov, P., S. Khelladi, F. Ravelet, C. Sarraf, F. Bakir and P. Vertenoeuil (2016). Experimental study of aerated cavitation in a horizontal venturi nozzle. *Experimental Thermal and Fluid Science* 70, 85-95.

Yu, X., C. Huang, T. Du, L. Liao, X. Wu, Z. Zheng and Y. Wang (2014). Study of characteristics of cloud cavity around axisymmetric projectile by large eddy simulation. *Journal of Fluids Engineering* 136(5).

Yuan, W. Sauer, and H. Shnerr (2001), Modeling and computation of unsteady cavitation flows in injection nozzles: Mec. Ind., 383 - 394.

Zhang, A. M., P. Cui, J. Cui and Q. X. Wang (2015). Experimental study on bubble dynamics subject to buoyancy. *Journal of Fluid Mechanics* 776, 137-160.

Zhang, X., W. Zhang, J. Chen, L. Qiu and D. Sun (2014). Validation of dynamic cavitation model for unsteady cavitating flow on NACA66. *Science China Technological Sciences* 57, 819-827.

Zwart, P. J., A. G. Gerber and T. A. Belamri (2004). Two- Phase Flow Model for Predicting Cavitation Dynamics, ICMF International Conference on Multiphase Flow.